Spin-layer coupling in two-dimensional altermagnetic bilayers with tunable spin and valley splitting properties

Yunxi Qi [1], Jun Zhao [1,*] and Hui Zeng [2,†]

[1] *Jiangsu Provincial Engineering Research Center of Low Dimensional Physics and New Energy & School of Science, Nanjing University of Posts and Telecommunications, Nanjing, Jiangsu 210023, China*

[2] *School of Microelectronics, Nanjing University of Science and Technology, Nanjing, Jiangsu 210094, China*

(Received 18 April 2024; accepted 10 July 2024; published 29 July 2024)

Recently, the discovery of collinear symmetric-compensated antiferromagnets (AFMs) with intrinsic spin splitting has attracted enormous interest of many researchers. In this paper, we predict the spin-layer coupling in altermagnetic bilayers with tunable spin and valley splitting properties via first-principles calculations. Based on the analysis of magnetic symmetry, we find manipulating magnetic order and stacking configuration as a strategy. Compared with conventional AFM bilayers, the joint symmetry in altermagnetic bilayer can be significantly modulated by different magnetic orders and stackings of the two sublayers. Furthermore, we demonstrate that the layer-dependent spin degeneracy/splitting widely exists in altermagnets with different crystal structures. The spin splitting in an altermagnetic bilayer with various interlayer couplings is highly tunable by external electric field. In contrast with spin splitting introduced by conventional spin-orbit coupling, the concepts of emerging layertronics and altermagnets are combined to manipulate spin properties by spin-layer coupling, ensuring both long spin relaxation time and complete spin splitting for practical applications of spintronic devices.

DOI: 10.1103/PhysRevB.110.014442

I. INTRODUCTION

Antiferromagnetism (AFM) has become a promising candidate for spintronic devices due to its insensitivity to external fields and ultrahigh dynamic velocity [1]. The AFM materials have multiple sublattices with complementary local magnetic moments. Conventionally, spin splitting is considered absent in AFM because of compensated sublattices [2]. However, recent studies have revealed a magnetic type called an altermagnet, which is characterized by its zero net magnetic moment and spin-polarized electronic bands [3–5]. It is noticed that the spin splitting in altermagnets originates from the magnetic space group and is protected by crystal symmetry [6,7]. For instance, the two-dimensional (2D) monolayers of V_2Se_2O and Cr_2SO are predicated to be altermagnets with spin splitting electronic bands at their valleys [8,9]. Moreover, recent experimental observations have confirmed the spin splitting in altermagnets due to broken $\mathcal{PT}$ symmetry, in which $\mathcal{P}$ is spatial inversion symmetry and $\mathcal{T}$ is time-reversal symmetry [10–13]. The achievement of spin splitting in altermagnets without spin-orbital coupling (SOC) facilitates their practical applications for spintronic and thermal transport devices [14–16]. The valleys, preserved by time-reversal symmetry ($\mathcal{T}$) in traditional ferrovalley materials, are also identified in altermagnets, and they are protected by lattice symmetry [8]. Therefore, the valley splitting in altermagnetic materials can be obtained by applying a uniaxial strain or constructing a new magnetic order [17].

The layer degrees of freedom (df) in multilayer systems provide an opportunity to explore physics [18,19]. The interlayer coupling modulation through different magnetic orders and stacking configurations has been applied to some ferrovalley bilayers, such as VSi_2N_4 and VS_2 bilayers [20]. The magnetic orders and stacking configurations in bilayers are related to the $\mathcal{PT}$ symmetry. The spin/valley properties in 2D altermagnetic materials are expected to be tuned via interlayer coupling. Compared with a monolayered nanostructure, the out-of-plane component of a layer-dependent pseudospin corresponds to the electric dipole moment, which can be tuned by an external electric field [21,22]. Consequently, a bilayer with various interlayer couplings is anticipated to be sensitive to the vertical electric field. Manipulation of spin splitting in altermagnetic bilayers is still lacking, although various 2D altermagnet monolayers have been investigated [23,24].

In this paper, we demonstrate the spin-layer coupling effect in 2D altermagnetic bilayers, and their spin splittings could be modulated by four joint symmetries. We provide a detailed calculation based on density functional theory, and the computational details are shown in the Supplemental Material [25]. Taking the V_2Se_2O and V_2S_2O bilayers as examples, we demonstrate that their spin/valley are degenerate under type-1 magnetic ordering, and this degeneracy is protected by $\mathcal{PT}t$ and $\mathcal{M}_z\mathcal{U}t$ symmetries. In sharp contrast, the reduction of spin group symmetry leads to spin splitting in the Brillouin zone (BZ) under type-2 magnetic order between sublayers [26]. The valley/spin splitting under the above two magnetic orders can be highly tuned through an external electric field. Most importantly, such nonrelativistic spin-layer coupling widely occurs in magnetic bilayer systems. We further take the Janus Cr_2SO bilayer as an example to demon-

*Contact author: zhaojun@njupt.edu.cn
†Contact author: zenghui@njust.edu.cn

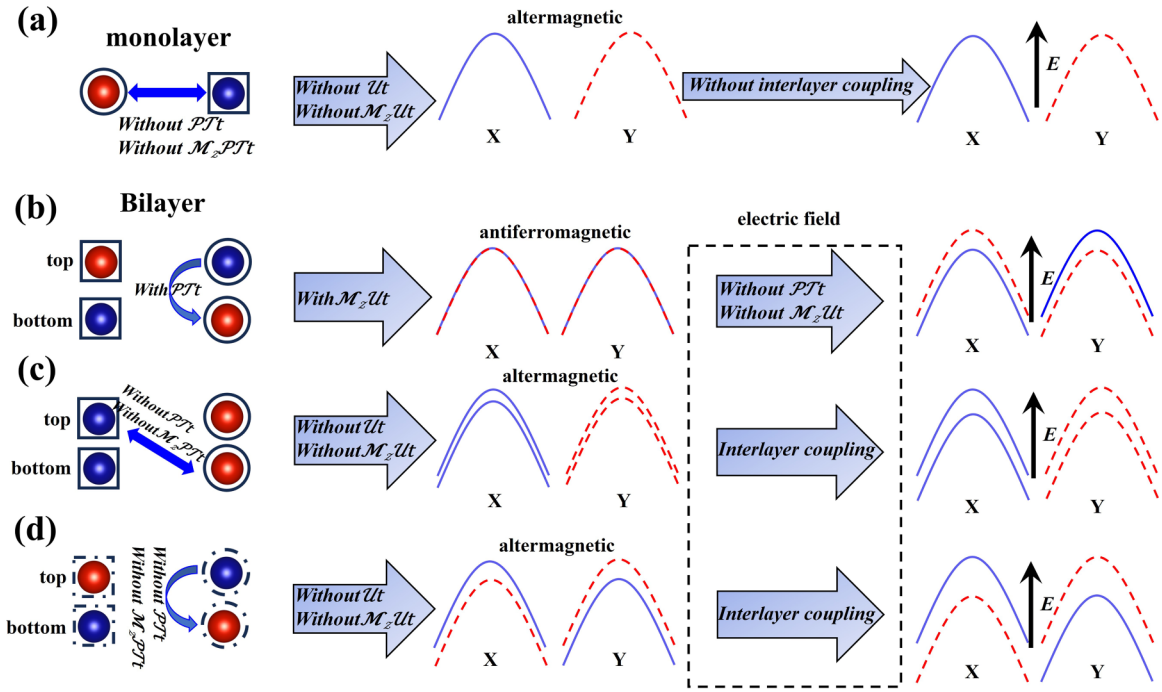

FIG. 1. Schematic diagram of (a) two-dimensional (2D) monolayer and (b)–(d) bilayer with various antiferromagnetic (AFM) exchange interactions. The red and blue solid balls represent the magnetic atoms with up and down magnetic moments, respectively. The solid (dash dotted) squares and circles indicate that the magnetic atoms have distinct coordination environments, and the same symbols represent the atoms in different sublayers are corrected by certain symmetries in real space. The magnetic atoms shown in (b) and (c), as indicated by solid squares (solid circles), in the top and bottom sublayers are coupled by $\mathcal{M}_z$ symmetries. In contrast, as shown in (d), the dash dotted squares reveal that the magnetic atoms in different sublayers cannot be coupled by $\mathcal{M}_z$ symmetry. The red dashed line and the blue solid line represent the spin-up and spin-down bands, respectively. The symbol E represents the presence of an external electric field, and the vertical black arrow represents the direction of the external electric field.

strate that the band degeneracy of an AA-stacked Cr_2SO bilayer with mirror symmetry is like that of the V_2Se_2O and V_2S_2O bilayers under two different magnetic orders. The spin degeneracy of the AA'-stacked Cr_2SO bilayer with mirror symmetry breaking is lifted in both magnetic orders, and the four joint symmetries of the top and bottom sublattices dominate the spin splitting at different k points in the BZ. Our theoretical investigation provides guidance to manipulate the spin splitting property in altermagnetic bilayer for practical applications [27].

II. SYMMETRY CONSIDERATIONS

In AFM crystals, the energy eigenvalues $E_\uparrow(k)$ are associated with $E_\downarrow(k)$ to generate fully spin-compensated bands, which originate from the $\mathcal{PT}$ symmetry contributed by two sublattices with opposite spins [28]. The $\mathcal{P}$ operation only reverses the vector k to produce $\mathcal{P}E_\uparrow(k) = E_\uparrow(-k)$, and the $\mathcal{T}$ operation reverses both k and spin σ to produce $\mathcal{T}E_\uparrow(k) = E_\downarrow(-k)$. Correspondingly, $\mathcal{PT}$ symmetry ensures $E_\uparrow(k) = \mathcal{PT}E_\uparrow(k) = E_\downarrow(k)$, resulting in spin-degenerate bands for two opposite components in the k space. There is also a simple translation (t) operation $tE_\uparrow(k) = E_\uparrow(k)$. Therefore, the energy eigenvalue of the AFM system that satisfies the $\mathcal{PT}t$ symmetry is $\mathcal{PT}tE_\uparrow(k) = E_\downarrow(k)$. In addition, the spin space and real space are completely decoupled when SOC is ignored, leading to a spin-reversal ($\mathcal{U}$) operation $\mathcal{U}E_\uparrow(k) = E_\downarrow(k)$, which is a spinor symmetric operation. Thus, the $\mathcal{U}t$ symmetry also ensures spin degeneracy at any wave vector k. For a 2D system, the wave vector k only has in-plane components. Therefore, the energy eigenvalues in a 2D system remain unchanged under planar mirror reflection $\mathcal{M}_z$ protection $\mathcal{M}_zE_\uparrow(k) = E_\uparrow(k)$.To generate spin splitting without SOC, it is essential to simultaneously break $\mathcal{PT}t$, $\mathcal{M}_z\mathcal{PT}t$, $\mathcal{M}_z\mathcal{U}t$, and $\mathcal{U}t$ symmetries [3,7,29].

Based on the above analysis, we consider a 2D tetragonal nanostructure, as shown in Fig. 1(a). In an altermagnetic monolayer, spin splitting originates from special magnetic space group. This magnetic structure breaks the $\mathcal{PT}t$, $\mathcal{M}_z\mathcal{PT}t$, $\mathcal{M}_z\mathcal{U}t$, and $\mathcal{U}t$ symmetries of spin-opposite sublattices. Additionally, the valleys in the tetragonal structure are protected by diagonal mirror symmetry $\mathcal{M}_\Phi$, suggesting that large valley polarization can be induced by uniaxial strain due to lattice symmetry breaking. However, the altermagnetic monolayers exhibit robust electronic structures to vertical external fields due to lacking of out-of-plane components for wave vector k. The altermagnetic bilayer with interlayer coupling is expected to be sensitive to an external field, as schematically shown in Fig. 1(b). The sublattices with different spin orientations in the top and bottom layers are correlated through joint symmetries, resulting in complete spin degeneracy like conventional AFM. The presence of an external electric field leads to the breaking of two joint symmetries, resulting in spin splitting. We define the magnetic order shown in Fig. 1(b) as type-1 magnetic order, that is, magnetic atoms in the top and bottom sublayers with opposite spins have the

same coordination environment. In contrast with the type-1 magnetic order, four joint symmetries are broken by changing the spin orientations of magnetic atoms in the top and bottom layers, resulting in spin splitting in altermagnetic bilayer. We thus could define type-2 magnetic order, as shown in Fig. 1(c). It suggests that the magnetic atoms in the top and bottom sublayers with opposite spins have different coordination environments. The valley/spin polarization in a bilayer can be easily tuned by strain to break the $\mathcal{M}_\Phi$ symmetry or by a vertical electric field to affect the interlayer coupling. To confirm our prediction, we further mediate the joint symmetry of the bilayer based on type-1 magnetic order while changing the coordination environment of magnetic atoms, as shown in Fig. 1(d). The mirror symmetry of the sublattices connecting the top and bottom sublayers is broken. Therefore, the absence of mirror symmetry leads to a built-in electric field between the two sublayers due to the electric dipole. This type of altermagnetic bilayer is expected to exhibit spin splitting independent of magnetic order, which is attributed to breaking four types of joint symmetry caused by the built-in electric field. The spin splitting of this stacking with both type-1 and 2 magnetic orders can be significantly tuned by interlayer coupling. Specifically, in the stacked bilayers with different magnetic orders, the joint symmetries of the spin-opposite sublattices in different sublayers dominate the spin splitting at different k points in momentum space, and the df of the layer is coupled with spin to form spin-layer locking. To verify the above prediction, we study several altermagnetic bilayers, including V_2Se_2O, V_2S_2O, and Cr_2SO bilayers, and different magnetic orders are considered to show the influences of spin-layer coupling to the spin-related properties.

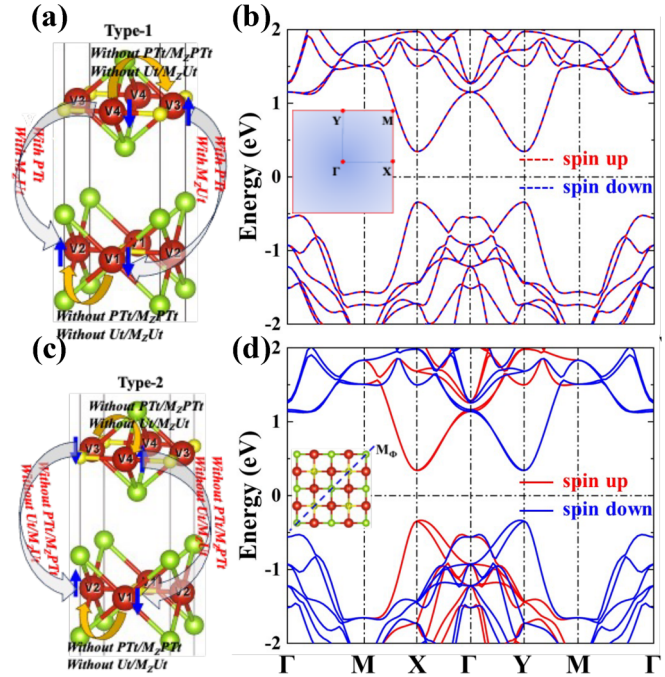

FIG. 2. The atomic structure and electronic bands of the A3 stacked V_2Se_2O bilayers with different magnetic orders. The (a) atomic structure of the type-1 magnetic order with symmetry operation denoted by the curved arrow, where the blue arrows indicate the direction of the magnetic moments of the V atoms. The (b) corresponding electronic structure of the type-1 magnetic order and the Brillouin zone (BZ) is shown in the inset, where the up and down arrows represent spin-up and spin-down components, respectively. (c) and (d) are the corresponding results of the type-2 magnetic order.

III. RESULTS AND DISCUSSION

We firstly take the V_2Se_2O bilayer as an example to demonstrate that its electronic structure is determined by interlayer coupling. The monolayered V_2Se_2O consists of an in-plane V_2O sandwiched by two Se planes. Our calculations have shown that its lattice constant is 3.91 Å, and its band structure agrees well with HSE06 functional calculation and previous reports when $U_{\text{eff}} = 4.7$ eV is used for the V atom, as shown in Fig. S1 in the Supplemental Material [25]. Both valence band maximum (VBM) and conduction band minimum (CBM) of the V_2Se_2O monolayer are located at X and Y points, forming two valleys protected by $\mathcal{M}_\Phi$ symmetry. The VBM and CBM of the V_2Se_2O monolayer are dominated by Se and V atoms, respectively. The V_2Se_2O monolayer is a semiconductor with a direct band gap of 0.68 eV. Owing to the opposite magnetic moments for the two V atoms, as schematically shown in Fig. 1(a), breaking four joint symmetries in a 2D monolayer leads to significant spin splitting in an altermagnet, as confirmed by Fig. S2 in the Supplemental Material [25]. It is noticed that the spin splitting is derived from AFM order with rotational operation τ to correlate the two magnetic atoms, rather than the SOC effect. Furthermore, the band structure including SOC shown in Fig. S2(a) in the Supplemental Material [25] demonstrates that the SOC effect is negligible [8].

For the V_2Se_2O bilayer, we consider four different stackings. The four types of different stackings are obtained by sliding the top sublayer relative to the bottom sublayer (detailed information is presented in the Appendix). For the A1 stacking, the V, Se, and O atoms in the top layer are directly above the V, Se, and O atoms of the bottom layer. Compared with the A1 stacking, the A2, A3, and A4 stackings are achieved by translating half of the length of the lattice constant along the a axis, diagonal, and b axis directions, respectively. Specifically, for the A2 and A4 stackings, the Se and O atoms in the top layer overlap with the two V atoms from the bottom layer, respectively. In the A3 stacking, the Se and O atoms in the top layer are directly located above the O and Se atoms in the bottom layer. We only consider the interlayer coupling of V_2Se_2O bilayers with AFM (i.e., type-1 and 2 magnetic orders), as the V_2Se_2O monolayer has an AFM Néel ground state [8,17].

The relevant parameters for the V_2Se_2O bilayers are shown in Table S1 in the Supplemental Material [25]. It is found that the total energy of the bilayer is related to the interlayer distance. The A2 and A4 stackings have similar total energies, and the A2 stacking has the largest total energy. In fact, A2 and A4 stackings can transform into each other through a C_4 symmetry operation of the bottom sublayer, leading to almost identical electronic properties. Among the four stackings, the A3 stacking has the lowest total energy and the smallest interlayer distance. We thus focus on the investigation of the V_2Se_2O bilayer with A3 stacking hereafter. Considering two magnetic orders shown in Figs. 2(a) and 2(b), our calculations reveal that the type-2 magnetic order is the ground state of

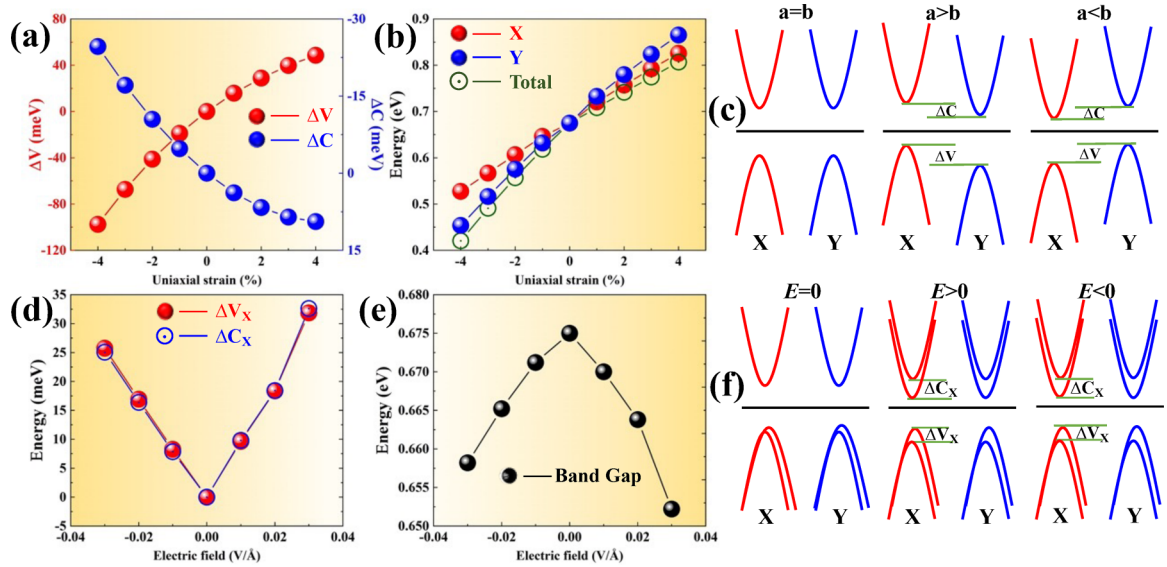

FIG. 3. In the A3 stacked V_2Se_2O bilayer with type-2 magnetic order, (a) the valley splittings for valence band (ΔV) and conduction band (ΔC) induced by uniaxial strain along the a axis, (b) the valley gaps at X and Y points and the total band gaps varied with respect to the uniaxial strain, and (c) schematic diagram of valley splitting. The solid red and blue lines represent the spin-up and spin-down bands, respectively. (d) The spin splittings for valence band (ΔV_X) and conduction band (ΔC_X) at the X point, and (e) total band gap, modulated by vertical electric fields. (f) Schematic diagram of the spin splitting. The solid red and blue lines represent the spin-up and spin-down bands, respectively.

the A3 stacking. Moreover, we find that the energy difference (ΔE) between type-1 and 2 magnetic order is around -2.3–1.2 meV, indicating weak interlayer magnetic coupling and the magnetic orders could be switched through magnetic proximity effect [30,31].

The atomic structure of the A3 stacking with type-1 magnetic order is shown in Fig. 2(a). The coordination environments of the magnetic atoms with opposite spins in the top and bottom sublayers are identical in the type-1 magnetic order. Specifically, the V_1 and V_3 (V_2 and V_4) atoms belonging to opposite spin sublattices are coupled with each other through the operations of $\mathcal{P}\mathcal{T}t$ and $\mathcal{M}_z\mathcal{U}t$. The electronic bands contributed by these two sublattices are degenerate, as shown in Fig. 2(b) and Fig. S3 in the Supplemental Material [25]. The bands contributed by the spin-down of the V_1 (V_4) atom and the band contributed by the spin-up of the V_3 (V_2) atom form doubly degenerated bands. When we only focus on the V_2Se_2O sublayer, i.e., V_1 and V_2 atoms are considered, the band contributed by each sublayer is spin splitting. The calculated result is like that of the V_2Se_2O monolayer, which is attributed to breaking of the four joint symmetries in 2D bilayer. As confirmed by Fig. S3 in the Supplemental Material [25], the bands contributed by the up-spin of the V_1 atom and the down-spin of the V_2 atom occupy the X and Y valleys, respectively, resulting in altermagnetic character with spin splitting bands. In contrast with the type-1 magnetic order between the two sublayers, the difference in the coordination environments of opposite spin sublattices leads to the breaking of four joint symmetries of dominant spin degeneracy, as demonstrated in Fig. 2(c). It leads to a spin splitting band like that of the V_2Se_2O monolayer, as evidenced by Fig. 2(d). Correspondingly, the spin-dependent electronic structures of the bilayer are determined by magnetic coupling between the two sublayers. The X and Y valleys are degenerate in energy for both type-1 and 2 magnetic orders for the V_2Se_2O bilayer, which is attributed to the protection of the $\mathcal{M}_\Phi$ symmetry. Hence, we show that the valley polarization can be generated by breaking the $\mathcal{M}_\Phi$ symmetry as a result of a uniaxial strain. Figure S4 in the Supplemental Material [25] shows that the band of the V_2Se_2O bilayer with the SOC effect is consistent with that omitting the SOC effect. As a result, we do not consider SOC in the following calculation.

Next, we discuss the modulation of spin/valley splitting by strain and external electric fields. For the V_2Se_2O monolayer, two nonequivalent valleys (X and Y points) are located at highly symmetric time-reversal invariant points in k space, and they are connected by crystal symmetry operations. Correspondingly, valley splitting of the V_2Se_2O monolayer can be achieved by using a uniaxial strain along the a or b axis to break the $\mathcal{M}_\Phi$ symmetry, which is confirmed by recent investigations [8]. We examine the evolution of the electronic structures of the bilayer by uniaxial strains, as exhibited in Fig. S5 in the Supplemental Material [25]. The valley splittings of the valence band (conduction band) are defined as the energy differences of the valence band (conduction band) at the X and Y valleys, respectively, which is computed by $\Delta V(\Delta C) = E^X_{V(C)} - E^Y_{V(C)}$. The valley splittings of the A3 stacked V_2Se_2O bilayer with type-2 magnetic order are summarized in Fig. 3(a). The $\Delta V(\Delta C)$ is found to be monotonically changed by the uniaxial strain. Specifically, a -4% uniaxial strain induces -97.5 and -24.7 meV valley splittings for ΔV and ΔC, respectively. The valley splitting value is larger than many 2D ferrovalley materials, such as VSCl (57.8 meV), LaBrI (59 meV), and VSSe (85 meV) [32,33]. Hence, the band gap of the V_2Se_2O bilayer can be substantially modulated by strain, as shown in Fig. 3(b). The band gap is monotonically increased with respect to the strain, which is like the previously report obtained for the

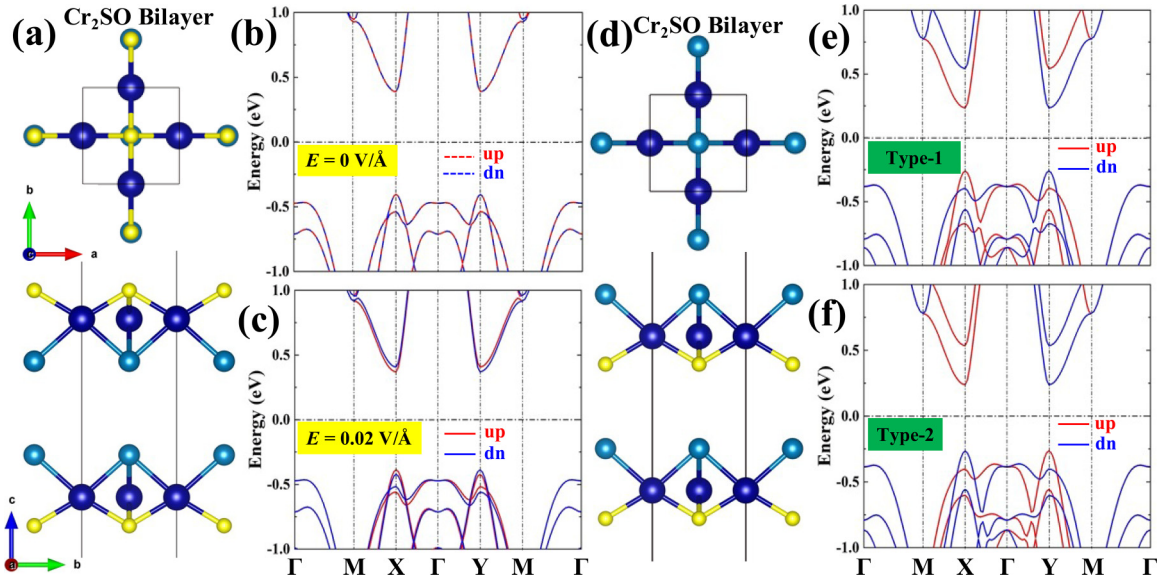

FIG. 4. (a) Top and side views of the atomic structure of the AA stacked Cr_2SO bilayers. The band structure of the Cr_2SO bilayer under type-1 magnetic order (b) without and (c) with an external electric field. (d) Top and side views of the atomic structure of the AA′ stacked Cr_2SO bilayers. The corresponding band structures of the Cr_2SO bilayer with (e) type-1 and (f) type-2 magnetic orders, where the red and blue lines represent the spin-up and spin-down bands, respectively.

Janus V_2SeTeO monolayer [17]. Furthermore, the interlayer coupling can be tuned by external electric field to induce prominent modifications on the electronic structure of the bilayer. As expected, both positive and negative electric fields induce band splittings for the VBM and CBM as a result of the Stark effect, as shown in Fig. S6 in the Supplemental Material [25] and schematically demonstrated in Fig. 3(f). We quantitatively define the VBM and CBM splittings at the X point as ΔV_X (energy difference between the highest and second-highest occupied bands) and ΔC_X (energy difference between the lowest and second-lowest unoccupied bands in the conduction band X valley). Figure 3(d) reveals that the band splittings are improved since the strength of electric field is enhanced. Therefore, the band gap of the bilayer is prominently reduced when the external electric field is increased.

Regarding to the A3 stacked V_2Se_2O bilayer with type-1 magnetic order, its valley degeneracy is also protected by $\mathcal{M}_\Phi$ symmetry. As shown in Fig. S7 in the Supplemental Material [25], the $\mathcal{M}_\Phi$ symmetry is broken by the uniaxial strain, leading to similar valley splitting properties to those of the type-2 magnetic order. Unlike conventional AFM monolayers, the spin degeneracy of the V_2Se_2O bilayers with type-1 magnetic order can be broken by external electric field. From the viewpoint of symmetry, vertical electric field causes an asymmetric charge distribution for the top and bottom sublayers, yielding the breaking of $\mathcal{PT}t$ and $\mathcal{M}_z\mathcal{U}t$ symmetries for the V_2Se_2O bilayer with type-1 magnetic order. Consequently, the presence of vertical electric field gives rise to tunable properties for the altermagnetic bilayer. We emphasize that such spin-layer coupling-related physical phenomena and valley-contrasting properties, relying on engineering layertronics, broadly exist in 2D altermagnetic bilayers. The V_2S_2O bilayer is confirmed to possess similar valley/spin physics, as shown in Fig. S8 in the Supplemental Material [25].

Furthermore, we propose that engineering layertronics relying on breaking different symmetries can be used to manipulate layer-spin locking and valley-contrasting properties, and this route can be generalized to many other 2D altermagnetic bilayers. Next, we consider the Janus altermagnetic Cr_2SO bilayer with low symmetry, as shown in Fig. 4, and AA and AA′ stackings are considered since the translation operation does not affect the joint symmetry of the crystal. The AA-stacked Cr_2SO bilayer maintains $\mathcal{M}_z$ and $\mathcal{P}$ symmetry. For the AA′ stacking, however, the $\mathcal{M}_z$ symmetry is broken. The spin degeneracy of the AA-stacked Cr_2SO bilayer with type-1 magnetic order is dominated by the Cr_1 and Cr_3 (Cr_2 and Cr_4) sublattices, and the Cr_1 and Cr_3 (Cr_2 and Cr_4) sublattices are coupled by $\mathcal{PT}t$ and $\mathcal{M}_z\mathcal{U}t$ symmetry, as shown in Figs. S9(a) and S10 in the Supplemental Material [25]. Thus, the spin-dependent band structure shown in Fig. 4(b) reveals that the bands are doubly degenerate due to the completely compensated spin sublattices. The $\mathcal{PT}t$ and $\mathcal{M}_z\mathcal{U}t$ symmetry can be further broken by a positive electric field, which gives rise to distinct spin splittings of the VBM and CBM at the X and Y valleys, as shown in Fig. 4(c). Moreover, type-2 magnetic order leads to the breaking of four joint symmetries, resulting in spin splitting and an altermagnetic character like that of the Cr_2SO monolayer [23], as evidenced by Figs. S9(b) and S11 in the Supplemental Material [25].

The above three examples illustrate that, for different altermagnetic bilayers with type-1 magnetic order, the spin degeneracy is dominated by the joint symmetry of opposite spin sublattices in different layers. However, in the case of the AA′-stacked Cr_2SO bilayer with type-1 magnetic order, its spin degeneracy is dominated by the joint symmetry of

opposite spin sublattices in the same layer. As shown in Fig. S12(a) in the Supplemental Material [25], the four joint symmetries of the Cr_1 and Cr_2 (Cr_3 and Cr_4) sublattices on the same layer are broken. As shown in Fig. 4(e) and Fig. S13 in the Supplemental Material [25], the lowest and second-lowest unoccupied states at the X and Y valleys are contributed by the top and bottom sublayers, respectively. Each sublayer exhibits a fully spin-polarized band like that of the altermagnet. Therefore, the breaking of symmetry of sublattices with opposite spins on the same layer dominates the spin splitting. In addition, a positive electric field of 0.03 V/Å leads to a significant enhancement of spin splitting ΔV_X to 391.4 meV compared with $\Delta V_X = 308.8$ meV in the absence of electric field, as presented in Fig. S14 in the Supplemental Material [25].

In the AA′-stacked Cr_2SO bilayer with type-2 magnetic order, as shown in Fig. S12(b) in the Supplemental Material [25] and Fig. 4(f), the corresponding electronic structure is very similar to the V_2Se_2O bilayer with type-1 magnetic order because four joint symmetries are broken. It is worth noting that, in conventional 2D AFM systems, such as the binary transition metal halides of $NiCl_2$ and CrI_3, the joint symmetry of their AFM bilayers cannot be broken by ordinary stacking or changing magnetic order due to the intrinsic spin degeneracy of the monolayer [29]. The intrinsic spin splitting and joint symmetry breaking of 2D altermagnetic monolayers provide a paradigm for spin control in AFM bilayer systems. Compared with conventional AFM bilayers with AFM property, the joint symmetry in altermagnetic bilayer is highly tunable and closely related to the interlayer coupling, which is expected to have more promising prospects for spintronic applications.

IV. CONCLUSION

In summary, we provide a simple approach to tuning spin splitting in 2D altermagnetic bilayers by simply changing the magnetic orders and stacking configurations, and the magnitude of spin splitting can be comparable with the SOC effect of heavy atoms. The spin degeneracy in 2D systems is protected by the joint symmetry of $\mathcal{P}\mathcal{T}t$, $\mathcal{M}_z\mathcal{P}\mathcal{T}t$, $\mathcal{M}_z\mathcal{U}t$, and $\mathcal{U}t$. Manipulation of magnetic orders and stacking configurations can break the joint symmetry, which is highly correlated with the layer df to achieve strong spin-layer coupling. Based on first-principles calculations, we demonstrate that layer-dependent spin degeneracy/splitting broadly exists in altermagnetic bilayers consisting of different crystal structures. Specifically, in sharp contrast with its monolayered counterpart, the spin polarization in an altermagnetic bilayer is highly tunable via interlayer coupling. Our theoretical proposal provides a generalized route to manipulate valley-related properties and spin splitting through tailoring layer stacking and interlayer coupling, facilitating practical application of spintronic devices based on 2D altermagnets.

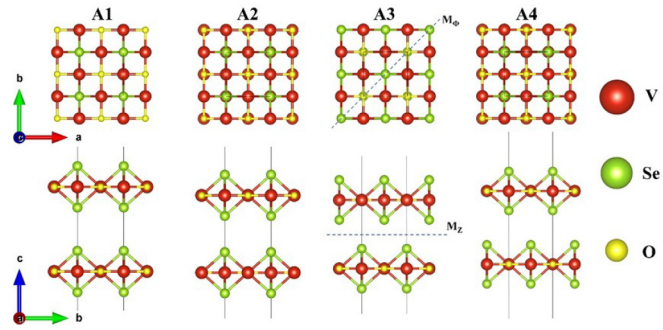

FIG. 5. Top and side views of the V_2Se_2O bilayer with different stackings, where red, light green, and yellow spheres represent V, Se, and O atoms, respectively. The light blue dashed line in the A3 stacking represents the diagonal mirror symmetry in the *ab* plane ($\mathcal{M}_\Phi$). The A1 stacking is obtained by AA stacking for the top and bottom sublayers. The A2 and A4 stackings are obtained by translating the bottom sublayer by $\vec{a}/2$ and $\vec{b}/2$ along the *a* and *b* axes, respectively. The A3 stacking is obtained by shifting the top sublayer by $(\vec{a}+\vec{b})/2$ along the diagonal direction.

ACKNOWLEDGMENTS

This work was supported by the National Natural Science Foundation of China (Grants No. 62174088 and No. 62371238). We are grateful to the High-Performance Computing Centre of Nanjing University for providing the IBM Blade cluster system.

APPENDIX: V_2Se_2O BILAYER IN DIFFERENT STACKINGS

We built the atomic structure of the V_2Se_2O bilayer with various different stackings. As shown in Fig. 5, the A1 stacking is obtained by AA stacking, that is, the top sublayer is exactly positioned above the bottom sublayer. The A2 and A4 stackings are obtained by translating the bottom sublayer by $\vec{a}/2$ and $\vec{b}/2$ along the *a* and *b* axes, respectively. The A3 stacking is obtained by sliding the top sublayer by $(\vec{a}+\vec{b})/2$ along the diagonal direction. The relevant structural parameters of the V_2Se_2O bilayer with different stackings are summarized in Table S1 in the Supplemental Material [25]. According to the calculated total energies of the V_2Se_2O bilayer with different stackings, the A3 stacking is the most energetically favorable nanostructure because it has the lowest total energy among the four stackings. As a consequence, we focus on the discussions of the A3-stacked V_2Se_2O bilayer and comprehensively study the influence of different magnetic orders on the electronic structure properties of the A3-stacked V_2Se_2O bilayer. Furthermore, it is found that the ground state of the A3-stacked V_2Se_2O bilayer is type-2 magnetic order, and the corresponding energy is slightly smaller (1.20 meV/cell) than that of the type-2 magnetic order.

[1] V. Baltz, A. Manchon, M. Tsoi, T. Moriyama, T. Ono, and Y. Tserkovnyak, Antiferromagnetic spintronics, Rev. Mod. Phys. **90**, 015005 (2018).

[2] T. Jungwirth, J. Sinova, A. Manchon, X. Marti, J. Wunderlich, and C. Felser, The multiple directions of antiferromagnetic spintronics, Nat. Phys. **14**, 200 (2018).

[3] L.-D. Yuan, Z. Wang, J.-W. Luo, E. I. Rashba, and A. Zunger, Giant momentum-dependent spin splitting in centrosymmetric low-z antiferromagnets, Phys. Rev. B **102**, 014422 (2020).

[4] L. Smejkal, R. Gonzalez-Hernandez, T. Jungwirth, and J. Sinova, Crystal time-reversal symmetry breaking and spontaneous Hall effect in collinear antiferromagnets, Sci. Adv. **6**, eaaz8809 (2020).

[5] R. González-Hernández, L. Šmejkal, K. Výborný, Y. Yahagi, J. Sinova, T. Jungwirth, and J. Železný, Efficient electrical spin splitter based on nonrelativistic collinear antiferromagnetism, Phys. Rev. Lett. **126**, 127701 (2021).

[6] L. Šmejkal, J. Sinova, and T. Jungwirth, Beyond conventional ferromagnetism and antiferromagnetism: A phase with nonrelativistic spin and crystal rotation symmetry, Phys. Rev. X **12**, 031042 (2022).

[7] L. Šmejkal, J. Sinova, and T. Jungwirth, Emerging research landscape of altermagnetism, Phys. Rev. X **12**, 040501 (2022).

[8] H.-Y. Ma, M. Hu, N. Li, J. Liu, W. Yao, J.-F. Jia, and J. Liu, Multifunctional antiferromagnetic materials with giant piezomagnetism and noncollinear spin current, Nat. Commun. **12**, 2846 (2021).

[9] X. Chen, D. Wang, L. Li, and B. Sanyal, Giant spin-splitting and tunable spin-momentum locked transport in room temperature collinear antiferromagnetic semimetallic CrO monolayer, Appl. Phys. Lett. **123**, 022402 (2023).

[10] S. Lee, S. Lee, S. Jung, J. Jung, D. Kim, Y. Lee, B. Seok, J. Kim, B. G. Park, L. Šmejkal *et al.*, Broken Kramers degeneracy in altermagnetic MnTe, Phys. Rev. Lett. **132**, 036702 (2024).

[11] J. Krempaský, L. Šmejkal, S. W. D'Souza, M. Hajlaoui, G. Springholz, K. Uhlířová, F. Alarab, P. C. Constantinou, V. Strocov, D. Usanov *et al.*, Altermagnetic lifting of Kramers spin degeneracy, Nature (London) **626**, 517 (2024).

[12] S. Reimers, L. Odenbreit, L. Smejkal, V. N. Strocov, P. Constantinou, A. B. Hellenes, R. Jaeschke Ubiergo, W. H. Campos, V. K. Bharadwaj, A. Chakraborty *et al.*, Direct observation of altermagnetic band splitting in CrSb thin films, Nat. Commun. **15**, 2116 (2024).

[13] Y.-P. Zhu, X. Chen, X.-R. Liu, Y. Liu, P. Liu, H. Zha, G. Qu, C. Hong, J. Li, Z. Jiang *et al.*, Observation of plaid-like spin splitting in a noncoplanar antiferromagnet, Nature (London) **626**, 523 (2024).

[14] D.-F. Shao, Y.-Y. Jiang, J. Ding, S.-H. Zhang, Z.-A. Wang, R.-C. Xiao, G. Gurung, W. J. Lu, Y. P. Sun, and E. Y. Tsymbal, Néel spin currents in antiferromagnets, Phys. Rev. Lett. **130**, 216702 (2023).

[15] X. Feng, H. Bai, X. Fan, M. Guo, Z. Zhang, G. Chai, T. Wang, D. Xue, C. Song, and X. Fan, Incommensurate spin density wave in antiferromagnetic RuO_2 evinced by abnormal spin splitting torque, Phys. Rev. Lett. **132**, 086701 (2024).

[16] X. Zhou, W. Feng, R.-W. Zhang, L. Šmejkal, J. Sinova, Y. Mokrousov, and Y. Yao, Crystal thermal transport in altermagnetic RuO_2, Phys. Rev. Lett. **132**, 056701 (2024).

[17] Y. Zhu, T. Chen, Y. Li, L. Qiao, X. Ma, C. Liu, T. Hu, H. Gao, and W. Ren, Multipiezo effect in altermagnetic V_2SeTeO monolayer, Nano Lett. **24**, 472 (2024).

[18] Z.-M. Yu, S. Guan, X.-L. Sheng, W. Gao, and S. A. Yang, Valley-layer coupling: A new design principle for valleytronics, Phys. Rev. Lett. **124**, 037701 (2020).

[19] D. Chen, Z. Lian, X. Huang, Y. Su, M. Rashetnia, L. Yan, M. Blei, T. Taniguchi, K. Watanabe, S. Tongay *et al.*, Tuning moire excitons and correlated electronic states through layer degree of freedom, Nat. Commun. **13**, 4810 (2022).

[20] X. Liu, A. P. Pyatakov, and W. Ren, Magnetoelectric coupling in multiferroic bilayer VS_2, Phys. Rev. Lett. **125**, 247601 (2020).

[21] Y. Shimazaki, M. Yamamoto, I. V. Borzenets, K. Watanabe, T. Taniguchi, and S. Tarucha, Generation and detection of pure valley current by electrically induced berry curvature in bilayer graphene, Nat. Phys. **11**, 1032 (2015).

[22] J. Lee, K. F. Mak, and J. Shan, Electrical control of the valley Hall effect in bilayer MoS_2 transistors, Nat. Nanotechnol. **11**, 421 (2016).

[23] S.-D. Guo, X.-S. Guo, K. Cheng, K. Wang, and Y. S. Ang, Piezoelectric altermagnetism and spin-valley polarization in Janus monolayer Cr_2SO, Appl. Phys. Lett. **123**, 028401 (2023).

[24] S.-W. Cheong and F.-T. Huang, Altermagnetism with noncollinear spins, npj Quantum Mater. **9**, 13 (2024).

[25] See Supplemental Material at http://link.aps.org/supplemental/10.1103/PhysRevB.110.014442 for the relevant parameters of the V_2Se_2O bilayer; the electronic bands of the V_2Se_2O monolayer obtained by HSE06 hybrid functional and different U_{eff} values; the electronic band and density of states of the V_2Se_2O monolayer under $U_{\text{eff}} = 4.7$ eV; four stacking structures and related parameters of the V_2Se_2O bilayer, the spin-projected electronic bands of the V_2Se_2O bilayer with type-1 magnetic order, and the evolution of their electronic bands and valley polarizations under different strains and electric fields; the spin-projected electronic bands of the V_2Se_2O bilayer with type-2 magnetic order and their electronic bands under different strains and electric fields; and the structure and related electronic bands of the V_2S_2O and Cr_2SO bilayers with different stackings and magnetic orders and their electronic bands influenced by electric fields, which includes Refs. [34–44].

[26] P. Liu, J. Li, J. Han, X. Wan, and Q. Liu, Spin-group symmetry in magnetic materials with negligible spin-orbit coupling, Phys. Rev. X **12**, 021016 (2022).

[27] T. Adamantopoulos, M. Merte, D. Go, F. Freimuth, S. Blügel, and Y. Mokrousov, Orbital Rashba effect as a platform for robust orbital photocurrents, Phys. Rev. Lett. **132**, 076901 (2024).

[28] S. Sheoran and S. Bhattacharya, Multiple Zeeman-type hidden spin splittings in $\mathcal{PT}$-symmetric layered antiferromagnets, Phys. Rev. B **109**, L020404 (2024).

[29] R. He, D. Wang, N. Luo, J. Zeng, K.-Q. Chen, and L.-M. Tang, Nonrelativistic spin-momentum coupling in antiferromagnetic twisted bilayers, Phys. Rev. Lett. **130**, 046401 (2023).

[30] G. Aivazian, Z. Gong, A. M. Jones, R.-L. Chu, J. Yan, D. G. Mandrus, C. Zhang, D. Cobden, W. Yao, and X. Xu, Magnetic control of valley pseudospin in monolayer WSe_2, Nat. Phys. **11**, 148 (2015).

[31] Y. Qi, C. Yao, J. Zhao, and H. Zeng, Tunable valley splitting in two-dimensional $CrI_3/MSi_2P_4 (M = \text{Mo, W})$ heterostructures: Interlayer coupling effects, Phys. Rev. B **108**, 125304 (2023).

[32] P. Jiang, L. Kang, Y.-L. Li, X. Zheng, Z. Zeng, and S. Sanvito, Prediction of the two-dimensional Janus ferrovalley material LaBrI, Phys. Rev. B **104**, 035430 (2021).

[33] C. Zhang, Y. Nie, S. Sanvito, and A. Du, First-principles prediction of a room-temperature ferromagnetic Janus VSSe monolayer with piezoelectricity, ferroelasticity, and large valley polarization, Nano Lett. **19**, 1366 (2019).

[34] G. Kresse and J. Furthmüller, Efficient iterative schemes for *ab initio* total-energy calculations using a plane-wave basis set, Phys. Rev. B **54**, 11169 (1996).

[35] G. Kresse and J. Hafner, *Ab initio* molecular dynamics for liquid metals, Phys. Rev. B **47**, 558 (1993).

[36] Y. Wang and J. P. Perdew, Correlation hole of the spin-polarized electron gas, with exact small-wave-vector and high-density scaling, Phys. Rev. B **44**, 13298 (1991).

[37] W. Kohn and L. J. Sham, Self-consistent equations including exchange and correlation effects, Phys. Rev. **140**, A1133 (1965).

[38] D. C. Langreth and M. J. Mehl, Easily implementable nonlocal exchange-correlation energy functional, Phys. Rev. Lett. **47**, 446 (1981).

[39] G. Kresse and D. Joubert, From ultrasoft pseudopotentials to the projector augmented-wave method, Phys. Rev. B **59**, 1758 (1999).

[40] H. J. Monkhorst and J. D. Pack, Special points for Brillouin-zone integrations, Phys. Rev. B **13**, 5188 (1976).

[41] S. Grimme, Semiempirical GGA-type density functional constructed with a long-range dispersion correction, J. Comput. Chem. **27**, 1787 (2006).

[42] J. Heyd, G. E. Scuseria, and M. Ernzerhof, Hybrid functionals based on a screened Coulomb potential, J. Chem. Phys. **118**, 8207 (2003).

[43] A. V. Krukau, O. A. Vydrov, A. F. Izmaylov, and G. E. Scuseria, Influence of the exchange screening parameter on the performance of screened hybrid functionals, J. Chem. Phys. **125**, 224106 (2006).

[44] K. Momma and F. Izumi, VESTA3 for three-dimensional visualization of crystal, volumetric and morphology data, J. Appl. Cryst. **44**, 1272 (2011).